EartharXiv – Submission Coversheet.

Title: Wildfire house loss hazard mapping and fuel management scenario planning on a Tasmanian wildland-urban interface using radiant heat and firebrand exposure modelling

---

Authors:

Grant J Williamson (Fire Centre, School of Natural Sciences, University of Tasmania) grant.williamson@utas.edu.au

Mastodon Handle: @jimbob@aus.social

Amila Wickramasinghe (Hawkesbury Institute for the Environment, University of Western Sydney) a.wickramasinghe@westernsydney.edu.au

Stefania Ondei (Fire Centre, School of Natural Sciences, University of Tasmania) stefania.ondei@utas.edu.au

Owen F Price (Fire Centre, School of Natural Sciences, University of Tasmania) of.price@utas.edu.au

David MJS Bowman (Fire Centre, School of Natural Sciences, University of Tasmania) david.bowman@utas.edu.au

---

Wildfire house loss hazard mapping and fuel management scenario planning on a Tasmanian wildland-urban interface using radiant heat and firebrand exposure modelling

Grant J Williamson[1], Amila Wickramasinghe[2], Stefania Ondei[1], Owen Price[1], David MJS Bowman[1]

[1]Fire Centre, School of Natural Sciences, University of Tasmania, Hobart, Tasmania, Australia

[2]Hawkesbury Institute for the Environment, University of Western Sydney, Penrith, New South Wales, Australia

Correspondence to: Grant Williamson (grant.williamson@utas.edu.au)

Abstract

Globally, wildfire disasters are increasing in frequency through a combination of urban expansion into flammable wildlands and climate change. Accordingly, the wildland urban interface (WUI) is a crucial geographic domain for disaster risk reduction. Accurate mapping of wildfire house loss hazard is a basic requirement for effective wildfire risk management. We developed a novel geographic analytical framework for mapping wildfire house loss hazard based on exposure to radiant heat load and firebrand density constrained by the biophysical environment of individual properties including vegetation type, fuel load, topography, and likely fire weather. We created a radiant heat exposure model based on physical principles and developed a statistical firebrand exposure model derived from detailed fluid dynamics modelling of firebrand transport. Combining outputs from these models we estimate total number of houses vulnerable to wildfire house loss for the WUI of Hobart, Tasmania, an extremely fire prone Australian capital city. We found our hazard mapping was more spatially nuanced that current official Tasmanian bushfire hazard mapping that broadly delineates areas with 100 m proximity to bushland > 1 ha. Using our hazard mapping framework, we explored the potential benefits of shaded firebreaks and prescribed burning fuel treatment scenarios in reducing wildfire house loss hazard, finding that exposure to firebrands were more important than exposure to radiative heat, particularly at greater distances from the interface. Further, our analyses suggest that mechanical thinning of bushland to increase the distance from homes by 50 m, combined with reducing bushland fuel loads by half, could substantially reduce by 68.3% the number of houses in mapped hazardous land (from 8,939 to 2,836 houses) in the study area. With acquisition of relevant fuel load and topographic inputs our wildfire house loss hazard mapping framework can be applied to flammable landscapes elsewhere in the world. Building on our findings and

previous research of garden wildfire hazards we propose a conceptual model of wildfire house loss hazard that can be used to further design wildfire house loss mitigation strategies on the WUI.

Keywords Forest fires, Fire breaks, Geospatial analyses, Embers, Firebrands, Natural hazard mapping, Wildfire Disaster

Introduction

The inexorable expansion of metropolitan areas into native wildlands driven by human population growth and population drift to urban areas has made the interface between fire-prone wildlands and urban areas (or wildland-urban interface (WUI)) the prime locus for economically disastrous wildfires (Hammer *et al.* 2007). The recent global increase in extreme fire weather has led to a corresponding marked escalation in wildfire disasters on the WUI with substantial loss of life and property (Abatzoglou et al., 2019; Anton & Lawrence, 2016; Caton et al., 2017; Chen et al., 2024; Cunningham et al., 2024, 2025; Jolly et al., 2015). The most economically destructive WUI wildfire disasters are concentrated in densely populated and affluent regions in temperate and Mediterranean biomes (Cunningham et al., 2025). Recent examples of these disasters in this biome include: the 2018 Camp Fire (18,800 structures lost) in California, USA (Knapp et al., 2021), the 2018 Attica fire (4,000 structures lost) in Greece (Molina-Terrén et al., 2019), the 2019-20 fires in NSW (2,475 houses) in Australia (Filkov et al., 2020), the 2024 Valparaiso fires (14,000 structures lost) in Chile (González et al., 2024) and the 2025 Los Angeles fires (16,000 structures lost) (Qiu et al., 2025).

Delineating the WUI is a critical approach for managing wildfire disaster risk through influencing building regulations and home insurance premiums as well as shaping fuel management programs. However, there remains little consensus on how to delineate this geographic construct at global, regional, and local scales. Typically, WUI mapping defines a buffer zone around flammable wildlands, albeit there is no agreement on the distance from wildland into urban areas. For instance, the WUI in the United States has been defined as areas with more than 6.17 buildings per km^2 and less than 50% wildland vegetation, located within 2.4 km of a large wildland patch (at least 5 km^2 in area and with more than 75% vegetation cover) (Carlson et al., 2022; Radeloff et al., 2005). By contrast, in Canada, research applied a WUI definition based on wildland fuel areas within a fuel-dependent buffer of a maximum distance of 2,400 m (Johnston & Flannigan, 2018), whereas in an Australian study from New South Wales, the WUI is defined as a 500 m buffer around urban areas with more than two properties per hectare (Price & Bradstock, 2013). Global analyses often follow the U.S. definition, and distinguish between 'Intermix' and

'Interface' WUI types, accounting for regional variations in vegetation and land use (Schug et al., 2023).

At regional to local scales distance to vegetation is commonly used as a proxy of radiant heat loading in wildfire house loss hazard mapping of WUI. For example, the Bushfire Prone Areas (BPA) broad planning overlays used by various Australian states is predicated the assumption that all forested land have equivalent radiant heat load that can be mitigated by a single fixed buffer distance (for example 100 m from forested areas). Place-based and property-level wildfire hazard assessments provide much finer granularity of wildfire hazard. In Australia, for instance, site-based assessments use physical equations to estimate the radiant heat load on the building given its distance to different vegetation types, terrain and fuel load (Standards Australia, 2011).

Despite the virtue of fine-grained modelling radiant heat, it must be admitted this approach does not adequately account for firebrands (or 'embers'), which pose significant wildfire risk at longer distances. Understanding firebrand dynamics and quantifying firebrand attack is important because house loss investigations have revealed that firebrands are the primary factor (Ramsay, 1995; Ramsay et al., 1987; Suzuki & Manzello, 2021). For example, investigations conducted after the 2003 Canberra fire indicated that over 90% of damaged houses were impacted solely by firebrands or the combined effects of firebrands and radiant heat (Blanchi et al., 2006; Leonard et al., 2004), while a Californian study surveying causes of building ignition from the 2007 Witch and Guejito fires found two thirds of ignitions were caused by firebrands (Maranghides & Mell, 2011).

Clearly an appreciation of both radiant heat and firebrands is essential for fine-scale mapping of wildfire house loss hazard on the WUI. Building on previous research (Leonard et al., 2014; Lowell et al., 2009; Wickramasinghe et al., 2023) we have developed a wildfire house loss hazard mapping framework encapsulated in an *R* software package that allows calculation of metrics of radiant heat exposure and firebrand exposure. We use this framework to: (a) estimate the number of properties in high wildfire house loss hazard (WHLH) areas in two highly fire prone local government areas (Hobart and Glenorchy) in southern Tasmania for a range of plausible fire weather scenarios; (b) contrast our wildfire hazard mapping with existing official wildfire hazard mapping based on the Tasmanian Government Bushfire Prone Areas (BPA) planning overlay; and (c) estimate reduction of houses in areas mapped as wildfire house loss hazard areas following a variety of fuel management treatments, including broadscale hazard reduction and targeted interface modification.

Methods

Study Area

The study was focused on two local government areas (City of Glenorchy and City of Hobart, Figure 1) that comprise the western shore of Hobart, the capital of the Australian state of Tasmania. The urban area of Hobart borders on the Wellington range, a significant topographic feature with a mix of wet and dry *Eucalyptus* forests that increase wildfire hazard on the wildland-urban interface. The urban fringe areas adjacent to and intermixed with forests are at risk of high intensity wildfires during extreme summer fire weather conditions, typified by strong, dry north-west winds enhanced by a Foehn effect (Grose et al., 2014). For example, the 1967 "Black Tuesday" fires that occurred under catastrophic fire weather impacted much of south-eastern Tasmania (Cheney, 1976) led to the loss of 1,293 buildings and 64 lives (Haynes et al., 2010).

We obtained the Bushfire Prone Area (BPA) boundary for both local government areas from Land Information System Tasmania's Planning Scheme Overlay (Tasmanian Planning Commission, 2024), noting that the boundary for the City of Hobart is still classified as interim due to ongoing planning reforms. This mapping is a statutory planning and building-control layer used by the Tasmanian Government to identify areas prone to bushfires, thereby guiding home construction based on a fixed proximity to defined flammable vegetation (100m), noting it does not consider fire behaviour, intensity, likelihood, or asset vulnerability. Vegetation mapping utilized the TasVeg 4.0 product (Tasmanian Department of Natural Resources and Environment, 2024), fuel loads were derived from database associated with the Tasmanian Fire Service fuel break guidelines (Tasmania Fire Service, 2024) and elevation from the Tasmanian 25m digital elevation model (Land Tasmania, 2024).

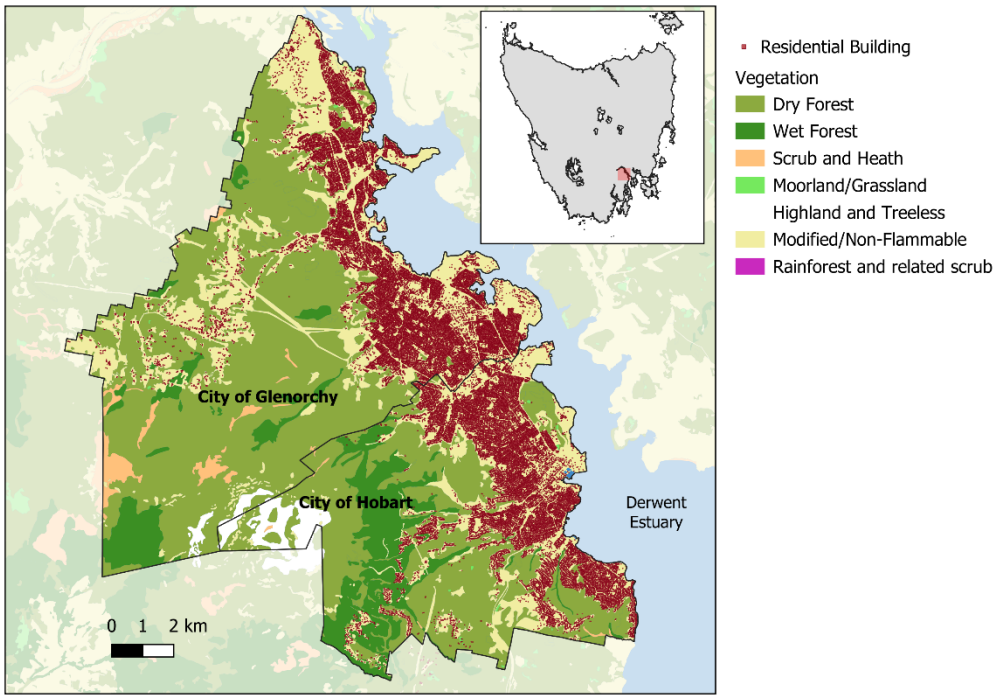

Figure 1 - Map of the two local government areas (City of Glenorchy and City of Hobart) that comprise the study area. Major vegetation types and residential building locations are indicated.

Radiant Heat Hazard Model

The Radiant Heat Hazard Model (RHHM), which estimates the radiant heat exposure of buildings, was based on an automated implementation of the Tasmanian Fire Service's (TFS) fuel-break width calculator, and has previously been used in the studies of Lucas et al. (2022) and Gjedrem et al., (2025) where it is briefly described. The RHHM calculates fireline intensity by implementing fire behaviour equations for a range of fuel types (grassland, forest, scrub and moorland) and management options (managed or unmanaged fuel), incorporating high (long-unburnt) fuel loads estimated for these vegetation communities, and the slope angle acquired from GIS thematic data (Tasmania Fire Service, 2024). The fuel-break width calculator then uses an iterative radiant heat flux model, as described in Hilton et al. (2020) and applied in AS-3959, to determine the minimum distance a building would need to be from the modelled fireline intensity in the specified vegetation type to achieve a radiant heat flux less than 12.5 kWm^2 (BAL-12.5). House exposure is then determined as the difference between the actual building distance from the vegetation, and the minimum safe distance, which will be negative for high-hazard properties.

In our RHHM methodology, we reimplemented the fuel-break width calculator algorithm in an R library (Williamson & Ellis, 2025) that incorporates an additional heuristic geographic algorithm to enable calculation of this minimum-hazard distance automatically for a set of residential properties, given suitable fuel and topographic input layers. To estimate radiant heat load for a

given input building, vectors are extended 150m outwards in the 8 cardinal directions, and along each vector, the vegetation type comprising the longest contiguous length is determined and assigned to that vector (Figure 2a). A maximum distance of 150m was chosen to ensure sampling encapsulated the maximum distance at which radiant heat is expected to impact houses for local vegetation types and fuel loads. Elevation values at points spaced 10m apart along each vector are extracted from a digital elevation model and a linear regression is performed on elevation versus distance. In cases where the linear regression has an R^2 value greater than 0.6, the slope angle is determined as the difference in elevation between the start and end points of the vector and an upslope or downslope status relative to the input point is defined, otherwise the vector is classified as being flat overall. In addition, a vector of distance 350m in the north-west direction is created, representing the likely direction of fire front approach in the study area under extreme fire weather (Atkinson et al., 2010). If the vector contains 300m of contiguous flammable vegetation, then the location is flagged as being potentially subject to the extreme fire behaviour associated with a fire run, as per the TFS fuel break width calculator algorithm (Tasmania Fire Service 2024). Attributes for each vector are then processed through the fire behaviour and radiant heat flux algorithm, and the length of the vector with the shortest safe distance from the fireline (e.g. maximum radiant heat flux) is selected to represent the hazard for the property. The actual distance of the building from the flammable vegetation is then subtracted from the estimated safe distance to generate a property hazard score, with negative values indicating the building is far enough away from the vegetation to receive a radiant heat flux of less than 12.5 kWm^2, while positive values indicate the building is too close to vegetation and would be exposed to a radiant heat flux greater than 12.5 kWm^2. The 12.5 kWm^2 value is a widely accepted threshold value above which houses are assumed to ignite due to radiant heat loading.

Numerical Firebrand Simulation

Building on the research of Wickramasinghe et al. (2023) we undertook numerical simulation of fire brands under a range of slope, fuel and fire weather conditions. Physical numerical simulations of firebrand generation, transport and landing were conducted in Fire Dynamics Simulator (FDS) version 6.9.1 in two model landscapes domains captured from LiDAR point clouds, with simulations covering a range of fire weather, fuel load, and topographic scenarios. Final modelled firebrand transport distances were used as the input for developing the empirical model of firebrand distance described in the next section. Detailed methods, scenarios, and grid sensitivity analysis for the numerical simulations are described in supplementary material sections S1 and S2.

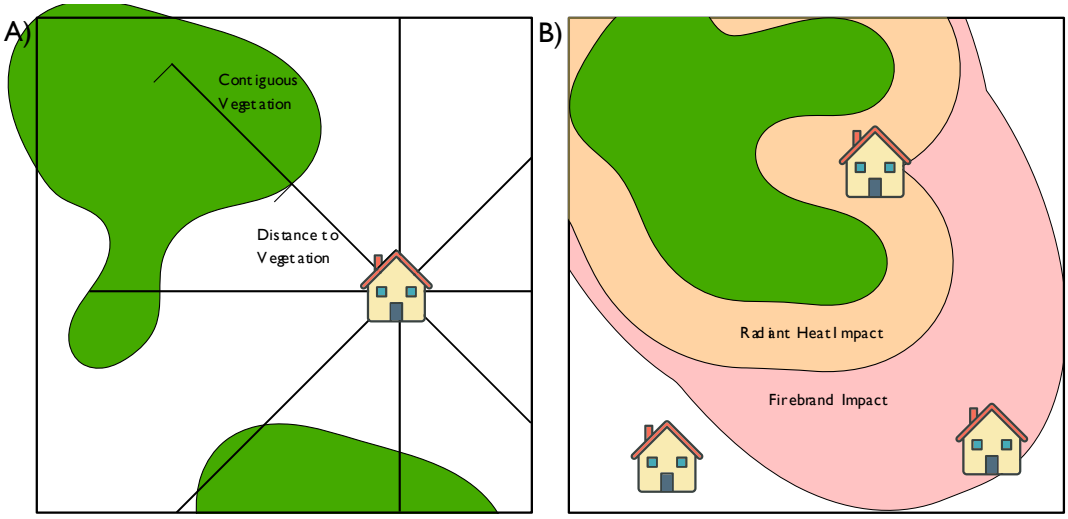

Figure 2 Conceptual model of the Radiant Heat Hazard Model (RHHM) used in this study, A) Determination of survivable distance (property receiving < 12.5 kWm^{-2}) from contiguous flammable vegetation along various cardinal directions through application of a radiant heat model. B) Example of combined radiant heat exposure and firebrand exposure zones extending from flammable vegetation area, with varying combinations of the hazards affecting houses through application of the RHHM and Statistical Firebrand Model.

Statistical Firebrand Model

The numerical simulations performed in the previous step produced a database of simulated landing distances for individual firebrands across the topographic, weather and fuel load scenarios. Across each scenario simulation domain, firebrand landings were binned onto a 5 m × 5 m grid and summarised along a set of Y-transects at 5 m spacing (42 transects for flat terrain and 7 transects for hilly terrain in each corresponding simulation); for each transect, the furthest downwind distance at which the firebrand density remained ≥ 5 firebrands m^{-2} was recorded (termed MD5) along with quantile distances (25th, 50th, 75th, 100th percentiles). These aggregated distances were used as the response variable in developing a statistical model of the limit of firebrand transport distance (MD5) as a function of fire weather, topographic and fuel conditions. A set of generalized additive quantile regressions (τ=0.95, n=2,250, Table 1) predicting log-transformed MD5 with combinations of surface fuel load (SFL), slope type (SLOPE) and a three-knot smooth of forest fire danger index (FFDI) were run, with the best performing model selected by Akaike's information criterion (AIC), and D^2 regression score as a fraction of pinball loss (Steinwart & Christmann, 2011) calculated as a measure of explanatory power. Quantile regression was selected to model firebrand transport distance because we were interested in how far the furthest firebrands travel rather than the average firebrand. Modelling was conducted in R version 4.5.1 (R Core Team, 2025), using the qgam (Fasiolo et al., 2021) package.

Table 1 - Quantile generalised additive models which were compared to develop the firebrand distance model.

Model name	Formula
Global Model	log(MD5) ~ s(FFDI [SLOPE]) + SFL + SLOPE
No Slope	log(MD5) ~ s(FFDI) + SFL
No Fuel	log(MD5) ~ s(FFDI [SLOPE]) + SLOPE
FFDI Only	log(MD5) ~ s(FFDI)
Null	log(MD5) ~1

Geographic Building Hazard Scenarios

In order to quantify and map hazard from radiant heat, firebrands, and additive hazard from both (Figure 2b), the radiant heat hazard model (RHHM) and statistical firebrand model (SFM) were run for each of 59,678 buildings in the Hobart and Glenorchy local government areas, with building data obtained from Land Information System Tasmania (Land Tasmania, 2020). Predictions of radiant heat exposure (above or below 12.5 kWm^2 at present vegetation distance) and firebrand exposure (greater than or less than 95^{th} quantile distance) were calculated at a range of forest fire danger index values from low to catastrophic (0 – 100). Building distance from vegetation is calculated from the vegetation edge which necessarily provides a high-end exposure estimate given the source proximity compared to radiant heat and firebrands produced deeper within the flammable vegetation. For each FFDI level, two fuel load scenarios were compared, the first using representative equilibrium fuel loads (based on Olson-curve parameters for Tasmanian fuel types) representing a scenario of no fuel management, for three broad vegetation groups common in the Hobart area, and the second using modified low fuel levels representing fuel-managed vegetation (Table 2) where equilibrium fuel loads have been divided in half.

Vegetation used for radiant heat and firebrand generation was based on TasVeg 4.0 vegetation mapping but with manual corrections incorporated for some areas that were classified as “urban/modified land”, but which still had extant forest cover on visual inspection of aerial photography. The case of typical summer fire weather conditions with a north-west wind (Smith, 1998) was assumed, with distance to firebrand generating vegetation only measured for vegetation patches in the north-west quadrant relative to each property.

Radiant heat and firebrand exposure were then simulated again in two additional scenarios, with vegetation removed in 25m or 50m buffers beyond the present vegetation boundary of properties that experienced radiant heat or firebrand exposure under the present vegetation configuration, to determine the relative hazard reduction achieved by additional fuel break development.

Table 2 – Fuel loads for three major vegetation types employed in spatial fire hazard model.

Vegetation Type	Equilibrium Fuel Load (t ha^{-1})	Low Fuel Load (t ha^{-1})
Dry Eucalypt Forest	14	7
Wet Eucalypt Forest	25	14
Non-Eucalypt Forest	13	6

Residential Building Exposure

Proportions of buildings exposed to radiant heat, firebrands, or both were plotted for the various fire weather, fuel load, and fuel clearance scenarios, in comparison to the proportion of buildings included within the present Bushfire Prone Areas definition, and the area of vegetation clearance required for the 25m and 50m buffer modifications calculated across the two local government areas.

Results

Radiant Heat Exposure

The radiant heat model produced an axiomatically pronounced exponential decline in radiant heat exposure with increasing distance from bushland. Using the radiant heat model, we identified 2,560 houses exposed of radiant heat exposure > 12.5 kWm^2 under severe (FFDI=50) fire weather in the two LGAs we studied. These houses are primarily around the WUI in close proximity to forest vegetation, and in semi-rural areas in the Wellington Range to the west of the urban area (Figure 3). The modelling also showed that radiant heat load increased in direct proportion to forest fire danger index (FFDI).

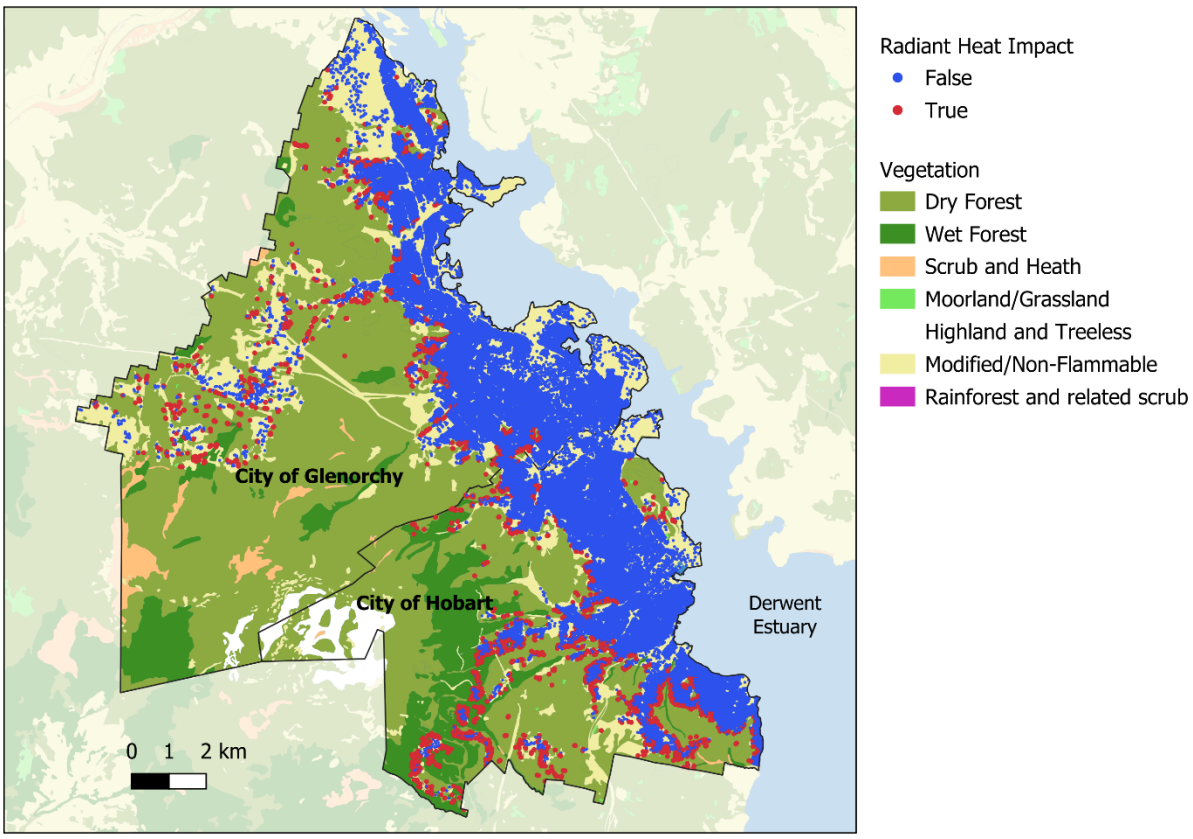

Figure 3 - Location of houses with radiant heat exposure of >12.5 kWm^{-2} under FFDI 50 conditions.

The modelling also showed the effect of fuel management interventions in reducing wildfire house loss hazard. Proportion of houses in the study area exposed to radiant heat (threshold 12.5 kWm^{2}) increased, as expected, with increasing fire weather index, and were greater under equilibrium fuel loads than reduced fuel loads (Figure 5A). Importantly, in all cases the proportion of buildings exposed was well below the proportion of buildings within the BPA zone. This, along with the rapid decrease in exposed for modified interfaces, with almost no houses affected by radiant heat when vegetation distance was increased by 50m, highlights the limited effect of radiant heat far from the interface, with most houses exposed being within the intermixed-interface zone, rather than past the linear urban interface.

Statistical Firebrand Exposure

Outputs of numerical simulations of firebrand landing distances showed upper quantile distances and spread of the landing distribution increasing with rising fire weather conditions, with greater distances associated with hilly landscapes and higher fuel load. Detailed results for the numerical simulations are provided in supplementary material section S3.

Using an operation definition of firebrand exposure (density >5 firebrands m^{-2}) our quantile regression modelling of firebrand transport distance identified the global model with fire weather,

fuel load, and slope type as predictors as the best performing, according to AIC rankings (Table 3). A marginal effect plot showing predictions with a surface fuel load of 25 t ha^{-1} shows an increase in firebrand transport distance with increasing fire danger, and more extreme distances (>400m at FFDI=100) for the hilly slope type, where firebrands are initiated at a higher elevation than the exposed properties (Figure 3).

Table 3 Statistical analysis maximum firebrand distance. AIC table of 95%ile quantile regression of maximum firebrand distance (density >5 firebrands m^{-2}) against fuel, topographic and fire weather variables, where MD5 is the maximum distance with a firebrand density. Columns show estimated degrees of freedom, log-likelihood, Akaike information criterion and delta from the top-ranked model. Percent deviance explained is reported, but is difficult to interpret for quantile regressions, so the alternative D^2 statistic is provided, which indicates how the model improves over the null model, on a scale of 0-1.

Model	Estimated DF	Log Link	AIC	dAIC	%DE	D^2
Global	7	-2502	5018	0	88.3	0.51
No Fuel	6	-2856	5724	706	87.2	0.47
No Slope	4	-4141	8290	3272	83	0.31
FFDI Only	3	-4262	8530	3512	81.7	0.271
Null	1	-5162	10326	5308	73.1	0

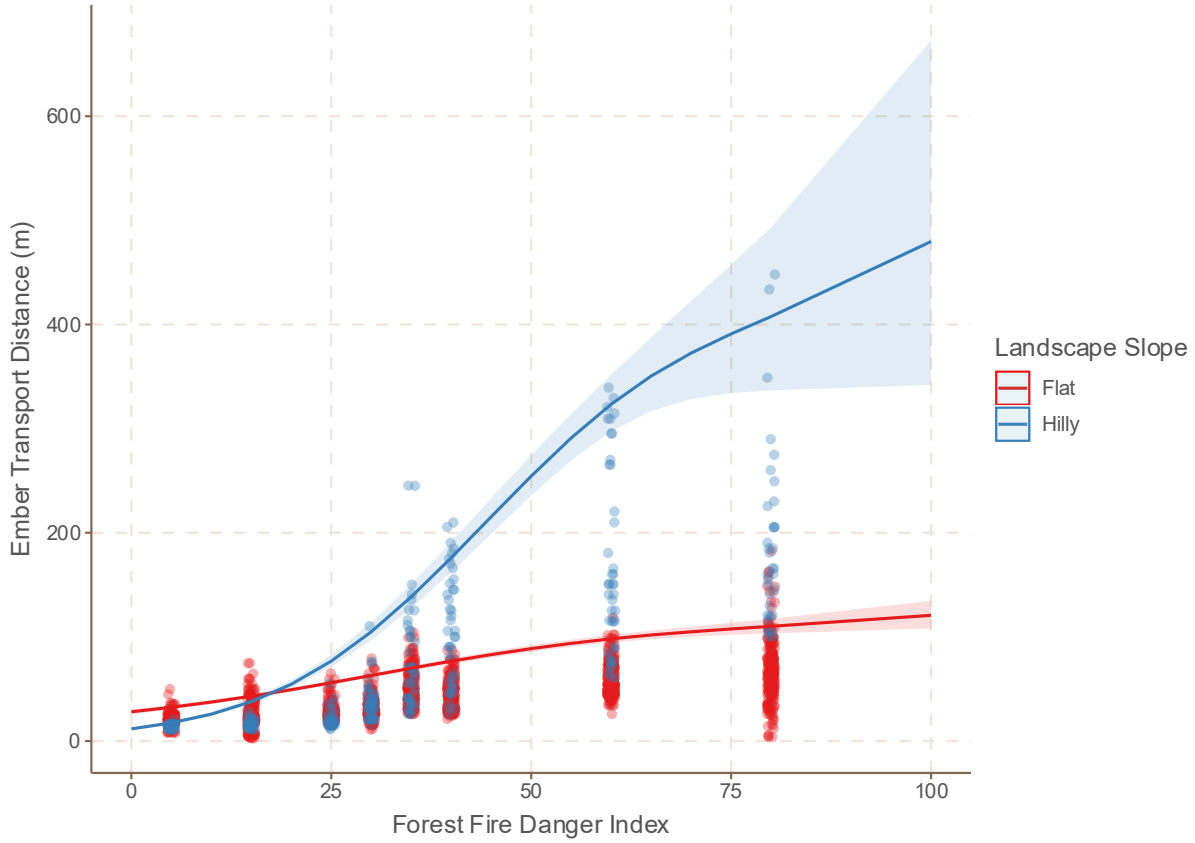

Figure 4 – Relationship of firebrand distances with fire weather for high (equilibrium) fine fuel loads. Marginal effects plot of maximum firebrand distance (density >5 firebrands m^{-2}) for a fuel load of 25 t ha^{-1} in flat and hilly landscape. Simulation distances are shown as dots, and 95th percentile quantile regression fits with 95% confidence intervals indicated by lines and shading.

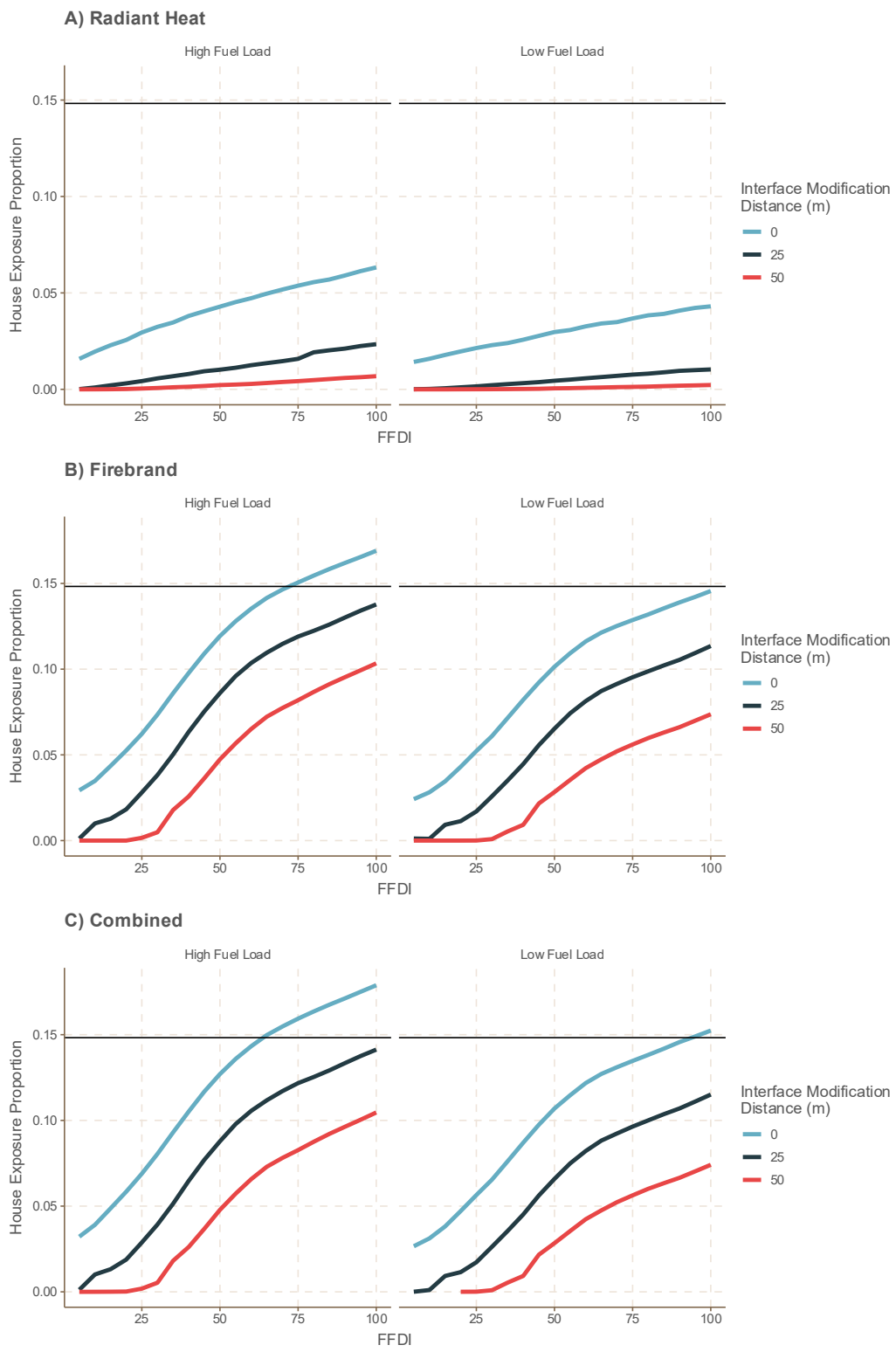

Figure 5 - House exposure to (A) radiant heat (> 12.5 kWm^2), (B) firebrand exposure and (C) additive combination of both for high and low fuel loads and modified interface distances across increasingly dangerous fire weather. Horizonal black line indicates the proportion of houses within the Bushfire Prone Area planning zone (n = 8,848, 14.8%).

Wildfire House Loss Hazard Mapping

Combined exposure from radiant heat and firebrand was used to assess wildfire house loss hazard for a range of management scenarios with increasing FFDI (Figure 5). In general, this combined exposure analysis showed very similar patterns to that of firebrand exposure (95^{th} quantile distance of MD5) alone (Figure 5B & 5C), with only a moderate increase in proportion of buildings at with high wildfire hazard, highlighting the limited radiant heat load on the majority of buildings that are located at greater distances from flammable vegetation (Figure 5A). The number of buildings in the official Bushfire Prone Area (BPA) classification (8,848) most closely matched the number of exposed buildings in our combined WHLH count (8,939) at an FFDI of 65. At this FFDI, 89.9% of houses had the same hazard classification under the BPA and our combined WHLH mapping, while 5% were considered exposed under BPA but not our method, and 5.1% were considered exposed under our method but not BPA (Table 4). Buildings classified as exposed under the BPA classification but not WHLH (Figure 6) tended to be in more semi-rural settings beyond the urban fringe, reflecting the tendency for the BPA zoning to cover broad areas, including houses even if they are within clusters of modified land. Buildings classified as exposed under our WHLH classification but not BPA tended to be on suburban fringe beyond the "first row", reflecting the stronger impact of more distant firebrand transport, and downwind of remnant vegetation patches excluded from the BPA classification, with particularly strong influence from forests on slopes above urban areas.

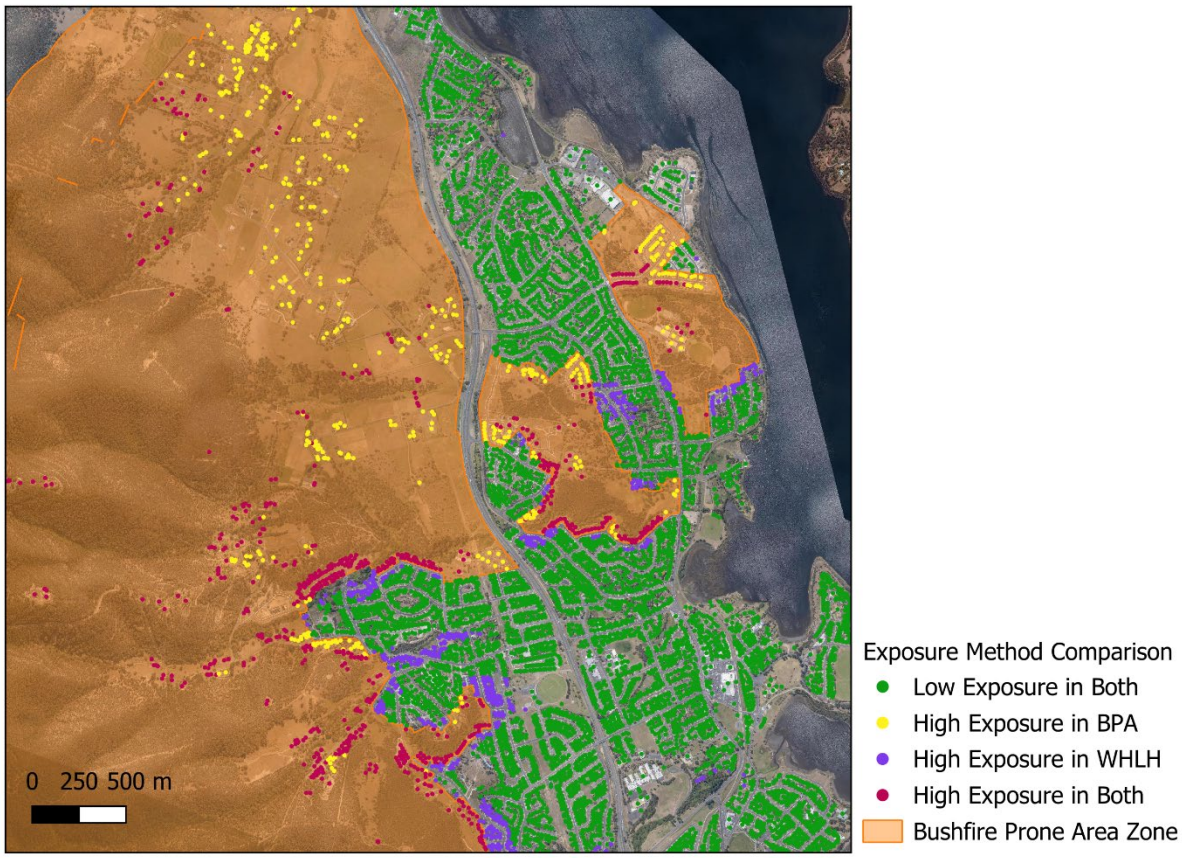

Figure 6 - Map of house exposure classification by BPL and WHLH methods for a region in the northern suburbs of Hobart, showing Bushfire Prone Area boundary.

Table 4 - Contingency table of building hazard classification based on Bushfire Prone Land (BPA) and our WHLH method, under the high fuel load, FFDI=65 scenario.

		Combined WHLH Exposure	
		False	True
Bushfire Prone Land Classification	False	47,774 (80%)	3,056 (5.1%)
	True	2,965 (5.0%)	5,883 (9.9%)

Summaries of the fuel management scenarios (high and low fuel loads, 0, 25 or 50m modified interface) at a set FFDI of 65 (severe) are shown in Figure 7. Maintaining vegetation fuel load at half the equilibrium level and expanding fuel breaks to establish additional 25m of clearance around high-hazard properties would reduce the proportion of homes by 41.1% (5,265 exposed homes compared to 8,939 in the default scenario). This additional 25m clearance, in the two local government areas in this study, would constitute 459ha of vegetation modification, while the more extreme 50m modification, which would reduce the number of homes by 68.3% (2,836

exposed homes), would equal 961ha. An example of the scale of interface modification around high-hazard properties tested in the scenarios is presented in Figure 8, noting that actual interface modification would have to be carefully guided to avoid sensitive vegetation and topographic conditions (for example, riparian vegetation).

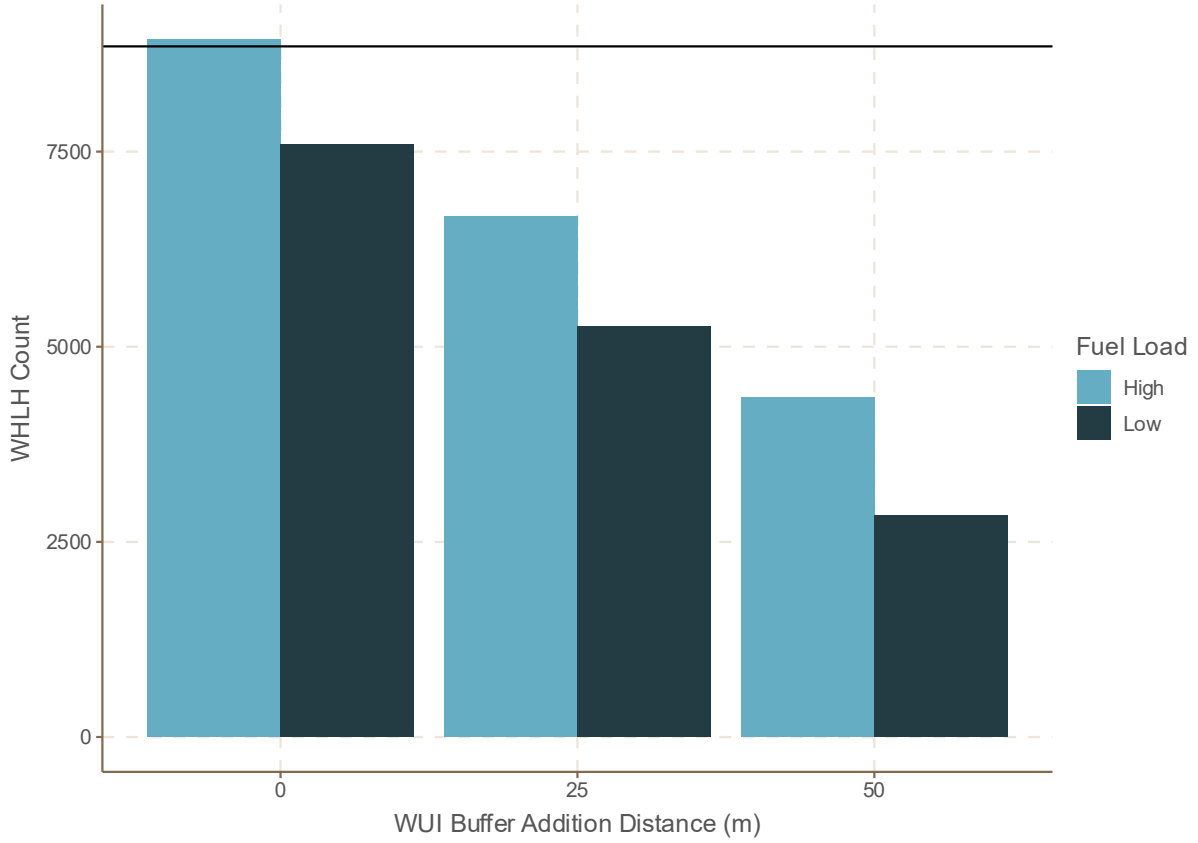

Figure 7 - Count of total houses with radiant heat or firebrand exposure for current interface distance (0m), and 25 and 50m increases in interface distance, for FFDI=65 (severe) fire weather conditions. Horizontal line shows count of buildings within Bushfire Prone Land (BPA) classification.

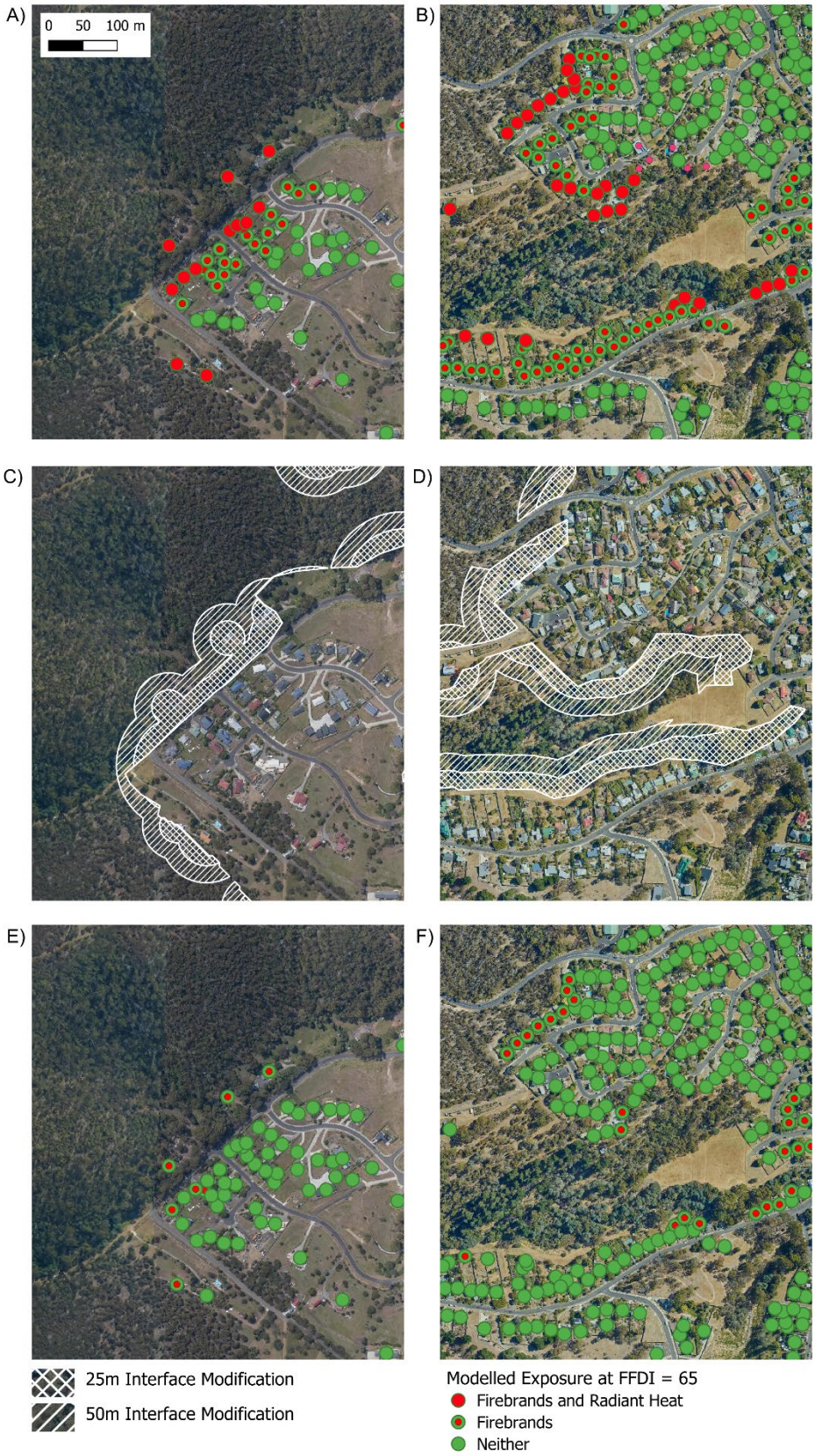

Figure 8 - Examples of the 25m and 50m interface modification buffers around high-hazard properties for areas of two suburbs in the study area, Montrose and Lenah Valley. Panels A and B show building exposure for the default scenario at an FFDI of 65, figures C and D shows 25m and 50m interface modifications applied in these

areas, and panels E and F show the resulting reduced exposure with a 50m increased interface and fuel management scenario applied.

Discussion

Mapping wildfire house loss hazard on the wildland urban interface (WUI) is a key for achieving sustainable coexistence with flammable landscapes because it enables targeted building designs, fuel management programs, and preparation for fire suppression campaigns. The simplest approach to mapping wildfire hazard on the WUI is to define it using thresholds based on geographic data of land cover and housing density (Chen et al. 2024). A variant of this approach is taken by Australian state governments in assessing wildfire hazard at broad geographical scales, identifying 'Bushfire Prone Areas'(Price & Bowman, In Review). More detailed mapping of wildfire hazard demands consideration of the complexity of fire behaviour, climate and fire weather, potential ignitions, fuel and flammability of landscapes, and vulnerability of the built environment to fire impacts. Such complexity has been assessed using a range of approaches including: laboratory and theoretical analyses (Catin et al. 2017), ensembles of wildfire simulation modelling (Bar Massada et al., 2009; Erni et al., 2024), machine learning (Miranda et al., 2020; Oliveira et al., 2021), geographic information system approaches (Atkinson et al., 2010; Herron et al., 2023; O'Connor et al., 2016), and frameworks linking incident-level simulations to structure impacts (Abo El Ezz et al., 2022). These approaches, however, are not practical for routine planning assessments across city to regional scales because of the demands of computational resources and the requirement for high-quality data. In this study we used a simpler and more pragmatic approach to estimate house loss hazard on the WUI using equations that estimate the fireline intensity (radiant energy) of a fire that spreads into the WUI (Lowell et al. 2009l Leonard et al. 2014). Such modelling applies fire behaviour equations using inputs for dangerous fire weather conditions and estimates of terrain variables and fuel loads derived from geographic information system data layers. This approach was bolstered by incorporating firebrands, which are a major factor affecting house loss on the WUI (Mell et al., 2010; Wickramasinghe et al., 2023).

Our approach to estimate radiant heat and firebrand exposure to underpin wildfire house loss hazard mapping represents an advancement over traditional methods, such as mapping 'Bushfire Prone Areas', which primarily rely on fixed buffer distances (for example, 100m from forest) and simplified assumptions about differences in vegetation flammability. By applying physics-based and statistical models at the property scale, we were able to quantify radiant heat

exposure and firebrand transport exposure under a range of fire weather and fuel scenarios, providing a more nuanced understanding of housing vulnerability across the interface. While our findings broadly align with regulatory Bushfire Prone Area (BPA) boundary radiant heat flux hazard patterns at severe fire weather conditions, it improves on this simple mapping scheme because it can capture local variations in radiant heat and firebrand exposure driven by topography, vegetation configuration, and prevailing wind direction. Particularly, we found that slope effects and the spatial orientation of vegetation relative to properties influence both radiant heat flux and firebrand transport, yet these factors are absent from the current 100 m buffer approach. Incorporating directional fire approach and terrain into hazard mapping clearly improves predictive accuracy. While our modelling here was applied specifically for Hobart, where a north-westerly direction of fire front approach is most likely for severe fire weather days (Atkinson et al., 2010), the methodology can be implemented in a more detailed manner that tests and weights multiple weather scenarios and fire approach directions. The regulatory BPA boundary for the regions of Hobart analysed identifies wildfire house loss exposure within broad areas of modified, agricultural, and pastoral land beyond the urban interface. Agricultural and grass fires are a somewhat distinct phenomenon from high-intensity forest fires, which have a higher fireline intensity and firebrand production mass than grasslands, but such rural grassland fires still pose a significant risk particularly associated with extreme wind storms (Balch et al., 2024). Inclusion of a distinct rural fire exposure model in our framework warrants further research and development.

The statistical firebrand model developed here offers a pragmatic alternative to computationally intensive physical simulations. This motivation is consistent with physics-aware exposure model of Roberts et al. (2021), who mapped community scale firebrand exposure using a computationally efficient 'ember load' metric derived from the spatial distribution of burned fine-fuel load and wind field, and showed a moderate association (Spearman's $\rho = 0.46$) with reported property damage in the 2015 Warringine Park bushfire while noting that outcomes also depend on factors not represented in the ember-load model (building materials and defensive actions by residents). Accuracy of such models could be enhanced through additional scenario testing across a broader range of weather conditions, to evaluate the separate importance of temperature and wind speed on firebrand generation and transport. Additional simulations in a wider range of landscapes with varying topographies would also allow for refining the slope–firebrand relationships we have developed (Figure 4), potentially establishing a continuous association that incorporates firebrand generation below house elevation.

A key insight from this analysis is the dominant role of firebrands in determining wildfire housing loss hazard within the WUI. Whereas radiant heat exposure declines rapidly with distance from flammable vegetation, following an inverse-square relationship and having greatest direct effect on houses in an intermixed interface, firebrand exposure persists over much greater distances, exhibiting a closer to linear decay. Consequently, firebrand attack poses a significant threat even to properties well beyond the immediate interface, underscoring the inadequacy of radiant heat–centric models and guidelines for comprehensive hazard assessment. This observation aligns with post-fire investigations that attribute the majority of house losses to firebrand ingress rather than direct flame contact (Ramsay, 1995; Ramsay et al., 1987). It should be noted that, due to uncertainties around the relationship between firebrand density and house loss probability, we selected an arbitrary reasonable threshold firebrand landing density (95^{th} quantile distance of 5 firebrands m^{-2}) but given the possibility of a single firebrand igniting a house we believe our exposure distance estimates are likely conservative. We expect that the more rapid distance drop-off of radiant heat compared to firebrands will hold for other selected threshold firebrand densities that may be established in future research.

Scenario fire management planning

The intervention scenarios explored in this study highlight the potential for targeted fuel management to substantially reduce wildfire house loss hazard. In one example scenario tested here, halving fuel loads and extending fuel breaks by 50 m around properties in high hazard areas could reduce radiant heat and firebrand exposure by almost 70% under severe fire weather conditions (Figure 6). Importantly, these interventions need not rely solely on traditional hazard reduction burning for fuel reduction, or "bare earth" fuel break construction; alternative strategies such as mechanical thinning, green or shaded fuel breaks (Curran et al., 2017; Murray et al., 2020), or managed woodland strips may achieve similar outcomes while preserving ecological and aesthetic values and maintaining social license (Bowman et al., 2018). However, given the potential for large trees to function as barriers to radiation and firebrands, further research is warranted to evaluate the effectiveness of these alternative approaches on both radiant heat attenuation and firebrand suppression.

While admittedly exploratory and anchored to one fire prone location (Hobart) the present approach provides a robust foundation for operational planning and policy development, emphasizing that effective WUI wildfire house loss hazard mitigation requires moving beyond simplistic buffer-based classifications, such as BPA mapping, toward property-specific hazard estimation. We acknowledge that the specific scenarios we tested used fixed spatial fuel loads. Our methodology could be refined by incorporating fire history and temporal fuel dynamics into

the inputs to more realistic wildfire house loss hazard mapping and fuel management scenario development.

Urban Conflagrations

Urban conflagrations are a profound and poorly understood peril of the WUI. Despite these advances, our models share a limitation with existing regulatory frameworks: they assume that wildfire threat originates exclusively from natural vegetation. In reality, however, once a fire penetrates the WUI, gardens and adjacent structures become primary sources of heat and firebrands, potentially transitioning the event into an urban conflagration. To date, the existing models of fire spread in urban fires (Hamada, M, 1951) and WUI fires (Chulahwat et al., 2022), do not that take full account of all the sources of wildfire hazard (natural vegetation, gardens, and buildings, (Price et al., 2025)). Future work should therefore integrate garden composition, property design, and house-to-house transmission dynamics into hazard models (Ondei et al., 2024, 2025), bridging the gap between landscape-scale hazard mapping and fine-scale vulnerability assessments. The connection between landscape scale hazard, as presented here, and garden and property scale hazards requires a linkage between the hazard type (radiant heat or firebrands) and the garden and property characteristics (Ondei et al., 2024). Such more complicated hazard mapping is required to reduce wildfire house loss hazard, for example changing garden design in areas in areas with high radiant heat and firebrand exposure.

Conceptual Model of WUI Hazard Reduction

We propose a framework for understanding wildfire house loss hazard reduction potential in the WUI based on the differing spatial scale and distance scaling of radiant heat and firebrand impact revealed in this study. In addition, we include the additional effects of garden and property design in enabling or preventing house-to-house spread within the urban area. Under “worse case” conditions (Figure 9A), exposure is extreme close to the interface due to the high contribution of firebrand and radiant heat impacts, and exposure declines only slowly into the urban area due to inappropriate property and garden design. By implementing lower flammability property and garden designs within the urban area, property-sourced exposure can be reduced, reducing wildfire hazard deeper within the urban area (Figure 9B). Implementing fuel hazard reduction in the wildland vegetation has the effect of lowering the exposure overall due to reduced radiant heat and firebrand production (Figure 9C), while modifying the interface to increase the distance to flammable vegetation in high-hazard areas has the effect of shifting exposure leftwards, further wildfire house loss hazard (Figure 9D).

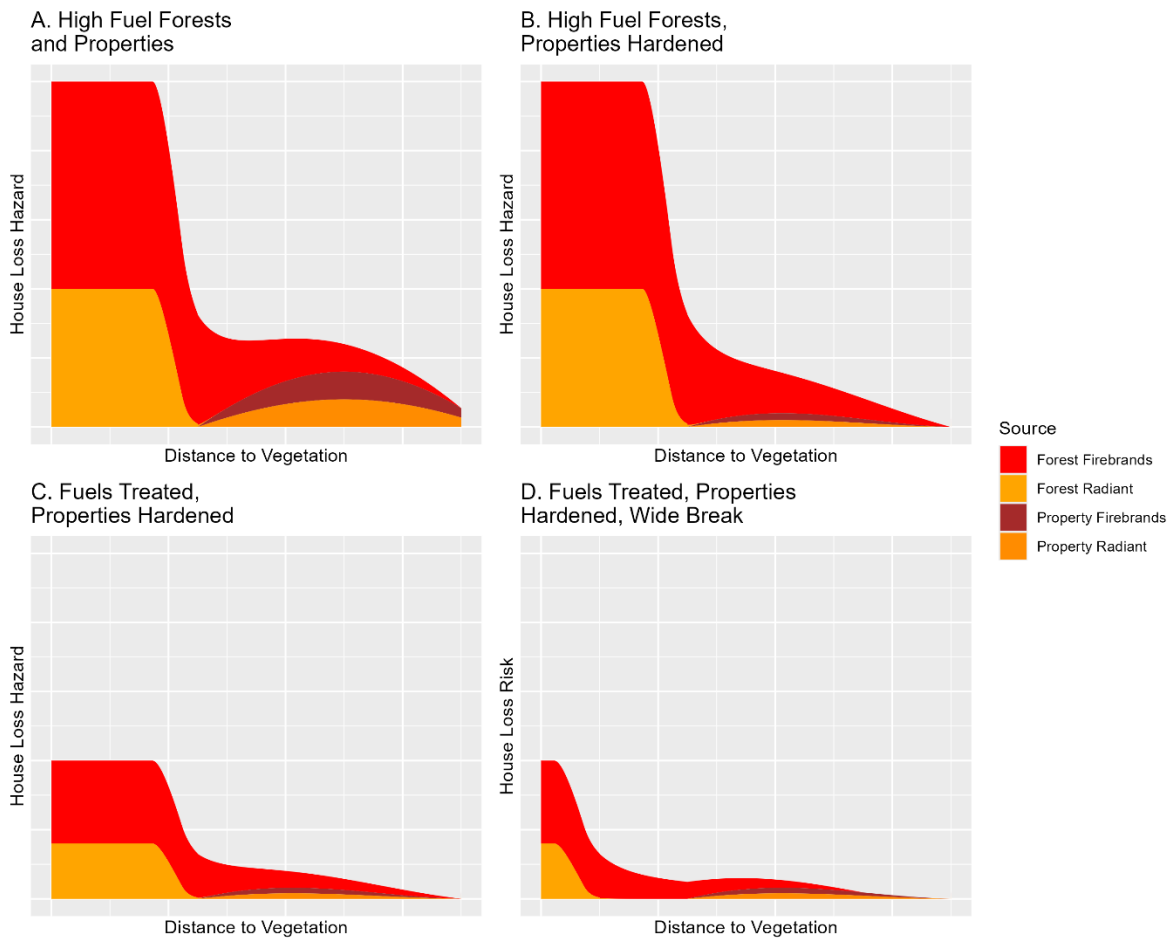

Figure 9 – Framework for wildfire hazard reduction in the WUI, showing relative contributions of various exposure factors that affect house loss hazard initiated by wildfires, incorporating sources of exposure from both wildlands and urban properties themselves, with increasing distance from the interface. Under the default scenario (A), better property and garden design (B), reduced forest fuel loads (C), and interface fuel break modification (D).

Based on this conceptual model we propose that the best return on wildfire hazard mitigation investments in the WUI should focus on the individual property-scale, reflecting the heterogeneity of housing vulnerability within the WUI rather than broadscale interventions based around complex definitions of the WUI. For example, Ondei et al. (2026) designed an approach to quantify key garden hazards (e.g. vegetation amount and connectivity) at broad scales using LiDAR data. This shift in spatial scale would enable more targeted and effective mitigation strategies and likely be easier to implement in a complex socioecological environment.

Further research is required to refine and test this conceptual model. Empirical analyses of actual house loss in past WUI fire events will provide critical insights into the drivers of structural failure and the relative importance of firebrand attack versus radiant heat. Incorporating detailed fire behaviour models would allow dynamic simulation of fire spread and intensity under varying

weather and fuel conditions provide validation data to improving predictive accuracy of geographic metrics such as we have developed. Addressing urban interface fire hazard also requires a deeper understanding of garden composition and design as contributors to ignition potential, given the role of ornamental vegetation and landscaping in sustaining fire within urban areas. Appreciation of how social attitudes to wildfire hazard mitigation strategies affect their social licence and uptake are required, and this will necessarily demand social science research including targeted behavioural economic analyses. Integrating diverse data streams—including vegetation mapping, building attributes, and socio-environmental and economic factors—into unified hazard models would bridge the gap between landscape-scale hazard mapping and property-level vulnerability assessment enabling practical pathways toward sustainable coexistence with wildfire on the WUI.

Conclusion

We have developed a novel geographic framework to assess wildfire house loss hazard on the WUI based on physical and statistical modelling of exposure to radiant heat and firebrand loads. We found that our mapping approach broadly aligns with current simple official mapping of Bushfire Prone Land (BPA) that is based on distance from flammable bushland. Our approach has greater sensitivity to terrain and fire weather variables than the spatially static BPA approach. Using the fire-prone WUI surrounding the city of Hobart as a case study to demonstrate our mapping provides an opportunity to evaluate the likely effectiveness of fuel treatment programs that reduce fuel loads and modify vegetation proximity to urban areas, a key innovation for wildfire mitigation planning design. Further, based on our findings and recent related research we have developed a simple conceptual model of the possible benefits of wildfire mitigation in both wildland (fuels and vegetation structure) and urban areas (gardens and houses). This conceptual model demands further investigation through targeted and carefully integrated research and development.

Acknowledgements and Funding

This work was funded by Australian Research Council Laureate Fellowship FL220100099 awarded to DMJSB. It was also funded and supported by Natural Hazards Research Australia project T2-A5: Bushfire risk at the rural-urban interface awarded to DMJSB, SO, OP and GJW.

References

Abatzoglou, J. T., Williams, A. P., & Barbero, R. (2019). Global Emergence of Anthropogenic Climate Change in Fire Weather Indices. *Geophysical Research Letters*, *46*(1), 326–336. https://doi.org/10.1029/2018GL080959

Abo El Ezz, A., Boucher, J., Cotton-Gagnon, A., & Godbout, A. (2022). Framework for spatial incident-level wildfire risk modelling to residential structures at the wildland urban interface. *Fire Safety Journal*, *131*, 103625. https://doi.org/10.1016/j.firesaf.2022.103625

Anton, C. E., & Lawrence, C. (2016). Does Place Attachment Predict Wildfire Mitigation and Preparedness? A Comparison of Wildland–Urban Interface and Rural Communities. *Environmental Management*, *57*(1), 148–162. https://doi.org/10.1007/s00267-015-0597-7

Atkinson, D., Chladil, M., Janssen, V., & Lucieer, A. (2010). Implementation of quantitative bushfire risk analysis in a GIS environment. *International Journal of Wildland Fire*, *19*(5), 649. https://doi.org/10.1071/WF08185

Balch, J. K., Iglesias, V., Mahood, A. L., Cook, M. C., Amaral, C., DeCastro, A., Leyk, S., McIntosh, T. L., Nagy, R. C., St. Denis, L., Tuff, T., Verleye, E., Williams, A. P., & Kolden, C. A. (2024). The fastest-growing and most destructive fires in the US (2001 to 2020). *Science*, *386*(6720), 425–431. https://doi.org/10.1126/science.adk5737

Bar Massada, A., Radeloff, V. C., Stewart, S. I., & Hawbaker, T. J. (2009). Wildfire risk in the wildland–urban interface: A simulation study in northwestern Wisconsin. *Forest Ecology and Management*, *258*(9), 1990–1999. https://doi.org/10.1016/j.foreco.2009.07.051

Blanchi, R., Leonard, J. E., & Leicester, R. H. (2006). Lessons learnt from post-bushfire surveys at the urban interface in Australia. *Forest Ecology and Management*, *234*, S139. https://doi.org/10.1016/j.foreco.2006.08.184

Bowman, D. M. J. S., Daniels, L. D., Johnston, F. H., Williamson, G. J., Jolly, W. M., Magzamen, S., Rappold, A. G., Brauer, M., & Henderson, S. B. (2018). Can Air Quality Management Drive

Sustainable Fuels Management at the Temperate Wildland–Urban Interface? *Fire*, *1*(2), 27. https://doi.org/10.3390/fire1020027

Carlson, A. R., Helmers, D. P., Hawbaker, T. J., Mockrin, M. H., & Radeloff, V. C. (2022). The wildland–urban interface in the United States based on 125 million building locations. *Ecological Applications*, *32*(5), e2597. https://doi.org/10.1002/eap.2597

Caton, S. E., Hakes, R. S. P., Gorham, D. J., Zhou, A., & Gollner, M. J. (2017). Review of Pathways for Building Fire Spread in the Wildland Urban Interface Part I: Exposure Conditions. *Fire Technology*, *53*(2), 429–473. https://doi.org/10.1007/s10694-016-0589-z

Chen, B., Wu, S., Jin, Y., Song, Y., Wu, C., Venevsky, S., Xu, B., Webster, C., & Gong, P. (2024). Wildfire risk for global wildland–urban interface areas. *Nature Sustainability*, *7*(4), 474–484. https://doi.org/10.1038/s41893-024-01291-0

Cheney, N. P. (1976). Bushfire Disasters in Australia, 1945–1975. *Australian Forestry*, *39*(4), 245–268. https://doi.org/10.1080/00049158.1976.10675654

Chulahwat, A., Mahmoud, H., Monedero, S., Diez Vizcaíno, F. J., Ramirez, J., Buckley, D., & Forradellas, A. C. (2022). Integrated graph measures reveal survival likelihood for buildings in wildfire events. *Scientific Reports*, *12*(1), 15954. https://doi.org/10.1038/s41598-022-19875-1

Cunningham, C. X., Abatzoglou, J. T., Kolden, C. A., Williamson, G. J., Steuer, M., & Bowman, D. M. J. S. (2025). Climate-linked escalation of societally disastrous wildfires. *Science*, *390*(6768), 53–58. https://doi.org/10.1126/science.adr5127

Cunningham, C. X., Williamson, G. J., & Bowman, D. M. J. S. (2024). Increasing frequency and intensity of the most extreme wildfires on Earth. *Nature Ecology & Evolution*, *8*(8), 1420–1425. https://doi.org/10.1038/s41559-024-02452-2

Curran, T., Perry, G., Wyse, S., & Alam, M. (2017). Managing Fire and Biodiversity in the Wildland-Urban Interface: A Role for Green Firebreaks. *Fire*, *1*(1), 3. https://doi.org/10.3390/fire1010003

Erni, S., Wang, X., Swystun, T., Taylor, S. W., Parisien, M.-A., Robinne, F.-N., Eddy, B., Oliver, J., Armitage, B., & Flannigan, M. D. (2024). Mapping wildfire hazard, vulnerability, and risk to Canadian communities. *International Journal of Disaster Risk Reduction*, *101*, 104221. https://doi.org/10.1016/j.ijdrr.2023.104221

Fasiolo, M., Wood, S. N., Zaffran, M., Nedellec, R., & Goude, Y. (2021). **qgam**: Bayesian Nonparametric Quantile Regression Modeling in *R*. *Journal of Statistical Software*, *100*(9). https://doi.org/10.18637/jss.v100.i09

Filkov, A. I., Ngo, T., Matthews, S., Telfer, S., & Penman, T. D. (2020). Impact of Australia's catastrophic 2019/20 bushfire season on communities and environment. Retrospective analysis and current trends. *Journal of Safety Science and Resilience*, *1*(1), 44–56. https://doi.org/10.1016/j.jnlssr.2020.06.009

Gjedrem, A. M., Ondei, S., Price, O. F., Williamson, G. J., & Bowman, D. M. J. S. (2025). Where the landscape meets the garden gate: Fire risk perception and garden adaptation in Tasmania's wildland–urban interface. *International Journal of Wildland Fire*, *34*(9), WF24213. https://doi.org/10.1071/WF24213

González, M. E., Syphard, A. D., Fischer, A. P., Muñoz, A. A., & Miranda, A. (2024). Chile's Valparaíso hills on fire. *Science*, *383*(6690), 1424–1424. https://doi.org/10.1126/science.ado5411

Grose, M. R., Fox-Hughes, P., Harris, R. M. B., & Bindoff, N. L. (2014). Changes to the drivers of fire weather with a warming climate – a case study of southeast Tasmania. *Climatic Change*, *124*(1–2), 255–269. https://doi.org/10.1007/s10584-014-1070-y

Hamada, M. (1951). On The Rate of Fire Spread. In *Disaster Research* (pp. 35–44). Nonlife Insurance Rating Organisation.

Haynes, K., Handmer, J., McAneney, J., Tibbits, A., & Coates, L. (2010). Australian bushfire fatalities 1900–2008: Exploring trends in relation to the 'Prepare, stay and defend or leave

early' policy. *Environmental Science & Policy*, *13*(3), 185–194. https://doi.org/10.1016/j.envsci.2010.03.002

Herron, M., Jalali, A., Roös, P. B., Sidiqui, P., & Duncan, E. (2023). Management of city vulnerability to bushfire risk using advanced GIS-based spatial tools. In *Resilient and Sustainable Cities* (pp. 553–567). Elsevier. https://doi.org/10.1016/B978-0-323-91718-6.00030-X

Hilton, J. E., Leonard, J. E., Blanchi, R., Newnham, G. J., Opie, K., Power, A., Rucinski, C., & Swedosh, W. (2020). Radiant heat flux modelling for wildfires. *Mathematics and Computers in Simulation*, *175*, 62–80. https://doi.org/10.1016/j.matcom.2019.07.008

Johnston, L. M., & Flannigan, M. D. (2018). Mapping Canadian wildland fire interface areas. *International Journal of Wildland Fire*, *27*(1), 1–14. https://doi.org/10.1071/WF16221

Jolly, W. M., Cochrane, M. A., Freeborn, P. H., Holden, Z. A., Brown, T. J., Williamson, G. J., & Bowman, D. M. J. S. (2015). Climate-induced variations in global wildfire danger from 1979 to 2013. *Nature Communications*, *6*. https://doi.org/10.1038/ncomms8537

Knapp, E. E., Valachovic, Y. S., Quarles, S. L., & Johnson, N. G. (2021). Housing arrangement and vegetation factors associated with single-family home survival in the 2018 Camp Fire, California. *Fire Ecology*, *17*(1), 25. https://doi.org/10.1186/s42408-021-00117-0

Land Tasmania. (2020). *Building Polygons* [Dataset]. https://www.thelist.tas.gov.au/app/content/data/geo-meta-data-record?detailRecordUID=e5753e25-78d4-4b33-b55b-4fb41a14b1c6

Land Tasmania. (2024). *LIST Tasmania 25 Metre Digital Elevation Model* [Dataset]. https://www.thelist.tas.gov.au/app/content/data/geo-meta-data-record?detailRecordUID=47b71113-a99d-4a9c-82c0-ba92c8313e79

Leonard, J., Blanchi, R., & Bowditch, P. (2004, May). *Bushfire impact from a house's perspective*. Bushfire 2004 - Earth Wind and Fire, Adelaide, South Australia.

Leonard, J., Opie, K., Newnham, G., & Blanchi, R. (2014). *A new methodology for State-wide mapping of bushfire prone areas in Queensland*. CSIRO.

Lowell, K., Shamir, R., Siqueira, A., White, J., O'Connor, A., Butcher, G., Garvey, M., & Niven, M. (2009). Assessing the capabilities of geospatial data to map built structures and evaluate their bushfire threat. *International Journal of Wildland Fire*, *18*(8), 1010. https://doi.org/10.1071/WF08077

Lucas, C. H., Williamson, G. J., & Bowman, D. M. J. S. (2022). Neighbourhood bushfire hazard, community risk perception and preparedness in peri-urban Hobart, Australia. *International Journal of Wildland Fire*, *31*(12), 1129–1143. https://doi.org/10.1071/WF22099

Maranghides, A., & Mell, W. (2011). A Case Study of a Community Affected by the Witch and Guejito Wildland Fires. *Fire Technology*, *47*(2), 379–420. https://doi.org/10.1007/s10694-010-0164-y

Mell, W. E., Manzello, S. L., Maranghides, A., Butry, D., & Rehm, R. G. (2010). The wildland—Urban interface fire problem—Current approaches and research needs. *International Journal of Wildland Fire*, *19*(2), 238. https://doi.org/10.1071/WF07131

Miranda, A., Carrasco, J., González, M., Pais, C., Lara, A., Altamirano, A., Weintraub, A., & Syphard, A. D. (2020). Evidence-based mapping of the wildland-urban interface to better identify human communities threatened by wildfires. *Environmental Research Letters*, *15*(9), 094069. https://doi.org/10.1088/1748-9326/ab9be5

Molina-Terrén, D. M., Xanthopoulos, G., Diakakis, M., Ribeiro, L., Caballero, D., Delogu, G. M., Viegas, D. X., Silva, C. A., & Cardil, A. (2019). Analysis of forest fire fatalities in Southern Europe: Spain, Portugal, Greece and Sardinia (Italy). *International Journal of Wildland Fire*, *28*(2), 85–98. https://doi.org/10.1071/WF18004

Murray, B. R., Brown, C., Murray, M. L., Krix, D. W., Martin, L. J., Hawthorne, T., Wallace, M. I., Potvin, S. A., & Webb, J. K. (2020). An Integrated Approach to Identify Low-Flammability Plant Species for Green Firebreaks. *Fire*, *3*(2), 9. https://doi.org/10.3390/fire3020009

O'Connor, C., Thompson, M., & Rodríguez Y Silva, F. (2016). Getting Ahead of the Wildfire Problem: Quantifying and Mapping Management Challenges and Opportunities. *Geosciences*, *6*(3), 35. https://doi.org/10.3390/geosciences6030035

Oliveira, S., Rocha, J., & Sá, A. (2021). Wildfire risk modeling. *Current Opinion in Environmental Science & Health*, *23*, 100274. https://doi.org/10.1016/j.coesh.2021.100274

Ondei, S., Price, O. F., & Bowman, D. M. J. S. (2024). Garden design can reduce wildfire risk and drive more sustainable co-existence with wildfire. *Npj Natural Hazards*, *1*(1), 18. https://doi.org/10.1038/s44304-024-00012-z

Ondei, S., Williamson, G., Foyster, S., & Bowman, D. (2026). Incorporating airborne LiDAR into reliable and scalable garden wildfire hazard assessments at the wildland–urban interface. *International Journal of Wildland Fire*, WF25218. https://doi.org/10.1071/WF25218

Ondei, S., Williamson, G. J., Foyster, S., & Bowman, D. M. J. S. (2025). An expert system to quantify wildfire hazards in gardens and create effective defensible space. *International Journal of Disaster Risk Reduction*, *121*, 105424. https://doi.org/10.1016/j.ijdrr.2025.105424

Price, O. F., & Bowman, D. M. J. S. (In Review). *Australian 2019-20 fire disaster house loss patterns confirm the reliability of the New South Wales Government bushfire risk mapping on the wildland-urban interface*.

Price, O. F., & Bradstock, R. A. (2013). The spatial domain of wildfire risk and response in the wildland urban interface in Sydney, Australia. *Natural Hazards and Earth System Sciences*, *13*(12), 3385–3393. https://doi.org/10.5194/nhess-13-3385-2013

Price, O. F., Ondei, S., & Bowman, D. M. J. S. (2025). Progress and prospects for predicting wildfire spread through the wildland-urban interface. *International Journal of Disaster Risk Reduction*, *121*, 105392. https://doi.org/10.1016/j.ijdrr.2025.105392

Qiu, M., Chen, D., Kelp, M., Li, J., Huang, G., & Yazdi, M. D. (2025). The rising threats of wildland-urban interface fires in the era of climate change: The Los Angeles 2025 fires. *The Innovation*, *6*(5), 100835. https://doi.org/10.1016/j.xinn.2025.100835

R Core Team. (2023). *R: A Language and Environment for Statistical Computing*. R Foundation for Statistical Computing. https://www.R-project.org/

Radeloff, V. C., Hammer, R. B., Stewart, S. I., Fried, J. S., Holcomb, S. S., & McKeefry, J. F. (2005). THE WILDLAND–URBAN INTERFACE IN THE UNITED STATES. *Ecological Applications*, *15*(3), 799–805. https://doi.org/10.1890/04-1413

Ramsay, G. C. (1995, September). *Building in the urban interface: Lessons from the January 1994 Sydney bushfires*. Bushfire'95, Australian Bushfire Conference, 27-30 September 1995, Hobart, Tasmania, Australia.

Ramsay, G. C., McArthur, N. A., & Dowling, V. P. (1987). Preliminary results from an examination of house survival in the 16 February 1983 Bushfires in Australia. *Fire and Materials*, *11*(1), 49–51. https://doi.org/10.1002/fam.810110105

Roberts, M. E., Rawlinson, A. A., & Wang, Z. (2021). Ember risk modelling for improved wildfire risk management in the peri-urban fringes. *Environmental Modelling & Software*, *138*, 104956. https://doi.org/10.1016/j.envsoft.2020.104956

Schug, F., Bar-Massada, A., Carlson, A. R., Cox, H., Hawbaker, T. J., Helmers, D., Hostert, P., Kaim, D., Kasraee, N. K., Martinuzzi, S., Mockrin, M. H., Pfoch, K. A., & Radeloff, V. C. (2023). The global wildland–urban interface. *Nature*, *621*(7977), 94–99. https://doi.org/10.1038/s41586-023-06320-0

Smith, D. T. (1998). *Mapping the bushfire danger of Hobart* [Honours]. University of Tasmania.

Standards Australia. (2011). *Construction of buildings in bushfire-prone areas* (3rd ed. reissued Incorporating Amendment Nos 1, 2 and 3). Standards Australia.

Steinwart, I., & Christmann, A. (2011). Estimating conditional quantiles with the help of the pinball loss. *Bernoulli*, *17*(1). https://doi.org/10.3150/10-BEJ267

Suzuki, S., & Manzello, S. L. (2021). Ignition Vulnerabilities of Combustibles around Houses to Firebrand Showers: Further Comparison of Experiments. *Sustainability*, *13*(4), 2136. https://doi.org/10.3390/su13042136

Tasmania Fire Service. (2024). *Fuel Break Width Calculator* [Computer software]. https://www.fire.tas.gov.au/Show?pageId=colFuelBreakCalculator

Tasmanian Department of Natural Resources and Environment. (2024). *TASVEG 4.0* [Dataset]. https://www.thelist.tas.gov.au/app/content/data/geo-meta-data-record?detailRecordUID=b5c7a079-14bc-4b3c-af73-db7585d34cdd

Tasmanian Planning Commission. (2024). *Tasmanian Interim Planning Scheme Overlay* [Dataset]. https://www.thelist.tas.gov.au/app/content/data/geo-meta-data-record?detailRecordUID=2d71412d-0c45-4d0d-942e-529a8aff425c

Wickramasinghe, A., Khan, N., Filkov, A., & Moinuddin, K. (2023). Physics-based modelling for mapping firebrand flux and heat load on structures in the wildland–urban interface. *International Journal of Wildland Fire*, *32*(11), 1576–1599. https://doi.org/10.1071/WF22119

Williamson, G., & Ellis, T. M. (2025). *Firekit* (Version 0.09) [R]. https://github.com/Fire-Centre/firekit

Supplementary Materials

S1 Firebrand Simulation Methods

To generate firebrand landing density (firebrands/m^2) and travel distance data under a range of fuel loads and fire-weather conditions, we employed a physics-based model, the Fire Dynamics Simulator (FDS) version 6.9.1 (McGrattan *et al.* 2013). Figure S1 illustrates the key processes involved in the physics-based modelling stage. We simulated Forest Fire Danger Index (FFDI) conditions of 5, 15, 25, 30, 35, 40, 60, and 80 by systematically varying wind speed and temperature inputs (Noble *et al.* 1980), representing fire danger categories from 'low-moderate' through to 'extreme'. The heat release rates were calculated according to the FDI and available fuel loads, as provided in AS-3959 (Australian Standard 2009) for forests, and were used as input parameters in the model. Fires were simulated in two case study domains: a topographically flat WUI (700m x 210m x 90m) affected by the Black Summer bushfires (2019-20), and a hilly WUI (800m x 50m x 180m) impacted by the Black Tuesday Hobart Fire (1967).

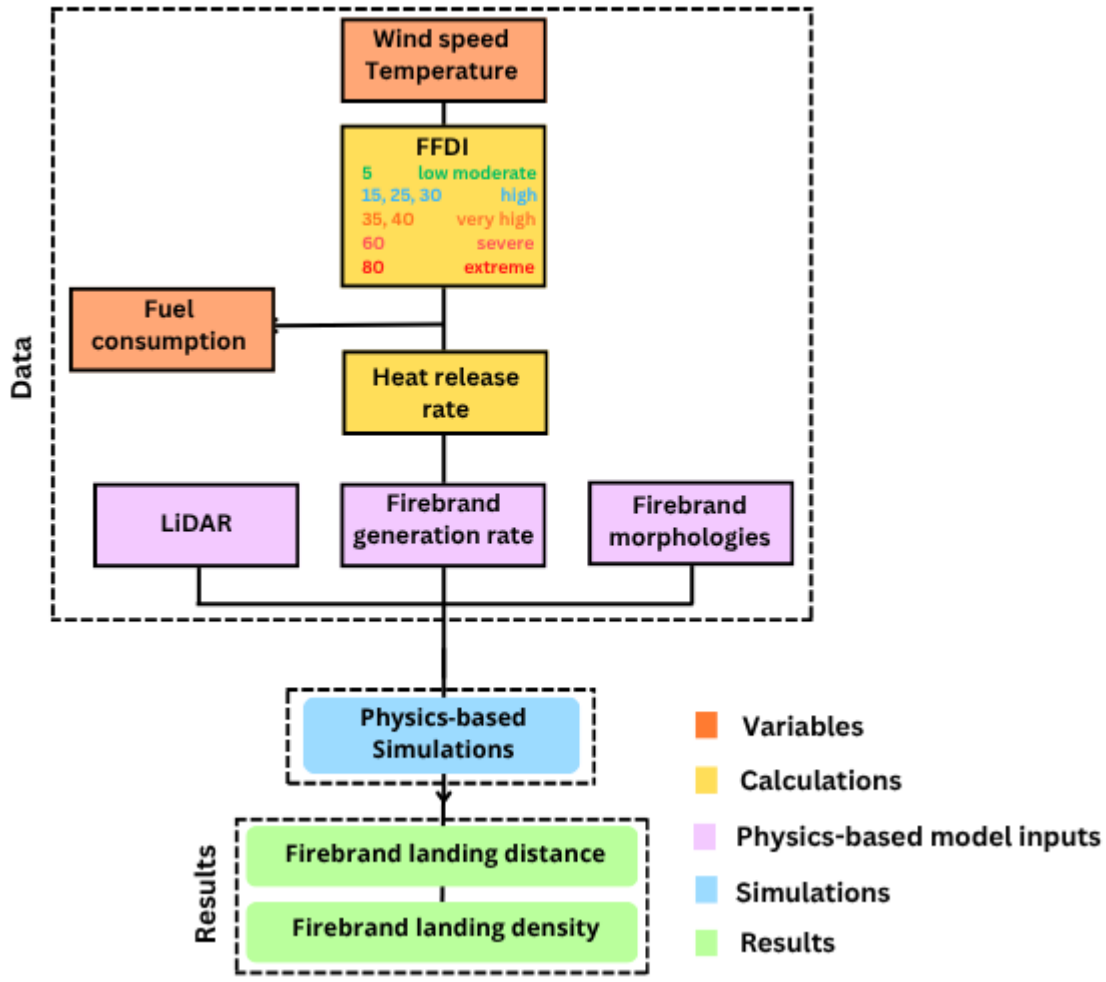

Figure S1 - The workflow outlines the key phases of the firebrand landing distribution analysis. In brief, either wind speed or air temperature was controlled to obtain the FFDIs, and the heat release rate of the fire line was calculated based on the FFDIs and fuel loads. LiDAR data was used to model housing layout, fuel structure, and terrain, replicating the interaction between wind flow, vegetation, and ground surface. The firebrands' generation rate and morphologies were inputs to the models. Firebrand landing distances and distributions were obtained to incorporate into statistical modelling to derive hazard zone buffer distances given fuel load and weather.

LiDAR data (Figure S2) sourced from (Geoscience Australia, 2024) enabled the representation of vegetation as a porous medium that interacts with the wind flow, creating a realistic near-ground flow field. The LiDAR point clouds of houses and the ground were modelled as solid obstructions, preventing wind and firebrands from passing through them. Firebrand input data, including size, shape, and composition, were derived from analysing images of firebrands collected from management-scale fires (El Houssami *et al.* 2016). The firebrands were generated within the volume of vegetation engulfed by the fire, with the generation rates (Table S1) maintained according to the heat release rate, as explained in (Wickramasinghe et al., 2022).

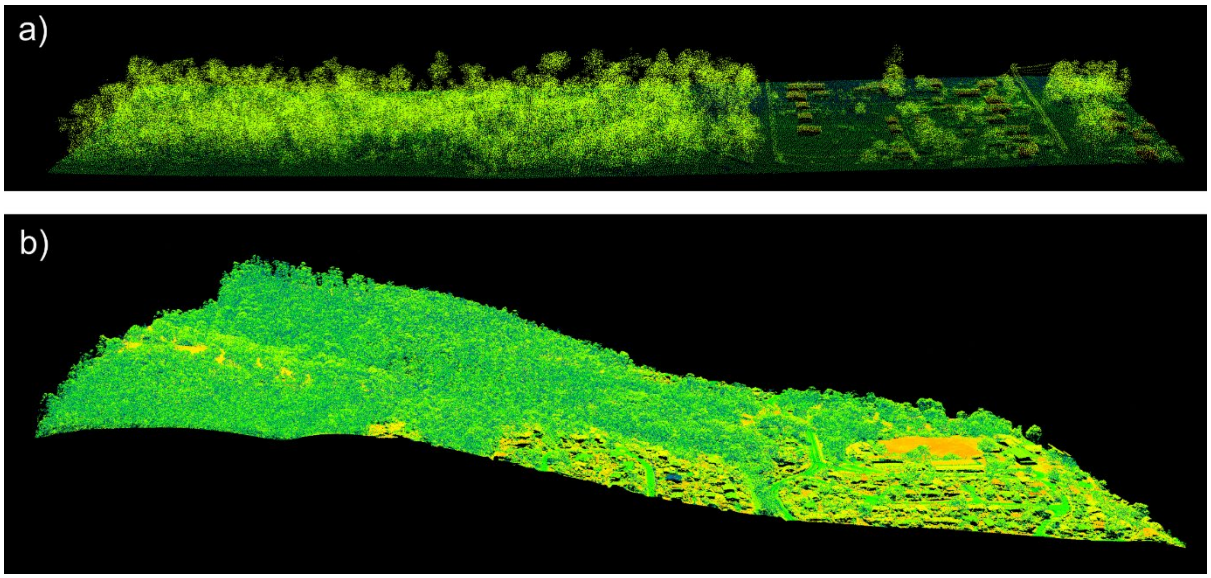

Figure S2 - LiDAR point cloud data for WUI sites: (a) Cann River, Victoria, a flat terrain affected by the 2019/20 Black Summer bushfire season, and (b) Taroona, Tasmania, a hilly region impacted by the 1967 Black Tuesday Hobart fire.36 simulations were conducted for each study area, using a 1-meter grid resolution, following a grid sensitivity analysis (Supporting Information S2), and utilizing parallel processing in a high-performance computing (HPC) facility (6,720 cores and 128 GM memory per node). The primary outcome of the simulations was the tracking of firebrand movement in space and time, accounting for the effects of wind drag, fire-induced buoyancy,

and their own weight. This allowed us to determine the landing distance and number of firebrands under the simulated fire-weather, vegetation and topography. For each simulation, we analysed 6-8 randomly placed transects (a total of 236), parallel to the wind field, along the downwind direction. For each transect, we calculated the maximum distance at which the landing density of firebrands dropped below 5 firebrands/m^2, which we refer to as MD5. This threshold was chosen because it is assumed that a firebrand landing density below this value is unlikely to lead to house ignition. While this threshold may be somewhat arbitrary, it is considered a more reliable measure than using the maximum landing distance, which could represent outlier or extreme firebrand events that unlikely causing an ignition.

Table S1 - Fireline intensity and firebrand generation rates used in physics-based simulations for varying FFDIs and fuel loads. These 18 different conditions were applied to flat and hilly landscapes separately, resulting in a total of 36 simulations.

Variables For FFDI	Wind speed (km/h)	Temperature (^{0}C)	Fuel load (t/ha)		FFDI	Fire Intensity (MW/m)	Firebrand generation rate (firebrands/MW/s)
			surface	Total			
Wind speed	5.0	41.1	17.5	24.5	5	1.33	0.59
	8.0	41.1			15	3.99	5.22
	13.0	41.1			25	6.64	10.00
	14.2	41.1			30	7.98	10.88
	15.5	41.1			35	9.3	11.74
	16.8	41.1			40	10.63	12.53
	34.1	41.1			60	15.95	19.52
	46.4	41.1			80	21.27	22.55
	5.0	41.1	25	35	5	2.71	0.59
	8.0	41.1			15	8.14	5.22
	13.0	41.1			25	13.56	10.00
	14.2	41.1			30	16.28	10.88
	15.5	41.1			35	18.98	11.74
	16.8	41.1			40	21.70	12.53

	34.1	41.1			60	32.55	19.52
	46.4	41.1			80	43.40	22.55
	5.0	41.1			5	3.78	0.59
	8.0	41.1			15	11.33	5.22
	13.0	41.1			25	18.89	10.00
	14.2	41.1			30	22.66	10.88
	15.5	41.1	29.5	41.3	35	26.43	11.74
	16.8	41.1			40	30.22	12.53
	34.1	41.1			60	45.33	19.52
	46.4	41.1			80	60.43	22.55
Temperature	7.0	10.0			5	1.33	5.96
	7.0	33.5			15	3.99	9.92
	7.0	48.6			25	6.65	10.66
	7.0	49.0			30	7.97	10.95
	40.0	21.5	17.5	24.5	35	9.3	9.97
	40.0	25.1			40	10.63	10.16
	40.0	37.1			60	15.95	10.78
	40.0	45.6			80	21.27	11.27
	7.0	10.0			5	2.71	5.96
	7.0	33.5			15	8.14	9.92
	7.0	48.6			25	13.56	10.66
	7.0	49.0			30	16.24	10.95
	40.0	21.5	25	35	35	18.99	9.97
	40.0	25.1			40	21.70	10.16
	40.0	37.1			60	32.55	10.78
	40.0	45.6			80	43.40	11.27
	7.0	10.0			5	3.78	5.96
	7.0	33.5			15	11.33	9.92
	7.0	48.6			25	18.89	10.66
	7.0	49.0			30	22.66	10.95
	40.0	21.5	29.5	41.3	35	26.44	9.97
	40.0	25.1			40	30.22	10.16
	40.0	37.1			60	45.33	10.78

	40.0	45.6			80	60.43	11.27

S2 Grid Sensitivity analysis

A grid sensitivity analysis was conducted using Grid Convergence Index (GCI) (Roy 2003; Ali *et al.* 2009), to identify an appropriate grid resolution for accurately capturing fire behaviour within the simulation domain. The GCI provides a quantitative estimate of numerical uncertainty associated with mesh refinement by quantifying how the solution changes across systematically refined grids, thereby indicating the degree of grid convergence. The GCI is calculated as:

$$GCI = F_S \frac{\epsilon_{rms}}{r^q - 1} \times 100 \qquad \textit{Eq. S1}$$

where q is the numerical scheme order, hence the value is 2 for the second-order scheme, and F_s is the factor of safety. The recommended value of F_s is in the range of 1.25 to 3 (Roy 2003), and r represents the grid refinement ratio that can be described as $r = (N_1/N_2)^{1/3}$, where N_1 and N_2 representing the number of cells in the finer and coarser grids, respectively. ϵ_{rms} is the root-mean-square value of the relative error that provides an initial measure of grid convergence for individual points. Grid resolutions of 0.75 m, 1.0 m, 1.5 m, and 2.0 m were evaluated based on the simulated wind speed, temperature, and heat release rate (HRR). Table S2 summarises the resulting GCI values for the U-velocity and temperature at selected locations within the domain.

Table S2. Grid convergence index (GCI,%) for different grid pairs for wind speed (U velocity component) and temperature at different locations within the domain

	Location	GCI (%)		
		(2.0 m/1.50 m)	(1.50 m/1.00 m)	(1.00 m/0.75 m)
Velocity	X=150 m	6.11	5.21	6.64
	X = 250 m	9.98	9.01	13.75
	X = 350 m	18.3	8.5	9.53
Temperature	X=450 m	52.02	16.97	25.26
	X = 550 m	16.81	6.06	18.63
	X = 650 m	10.61	7.58	11.56

Overall, the analysis indicates that a 1.0 m grid provides an effective balance between numerical accuracy, computational efficiency, and geometric representation of built features. This grid size maintained GCI values below 10% for most locations, meeting commonly accepted thresholds for CFD and fire modelling applications.

S3 Firebrand Simulation Results

The analysis of firebrand landing distances, as illustrated in Figure S3(a), reveals that the Q_{50} to Q_{95} distances increase with rising wind speeds under constant temperature and fuel load conditions, for both flat and hilly landscapes. This indicates that higher FFDI values are associated with greater firebrand landing distances. At the same wind speed, hilly landscapes show a greater firebrand travel distance compared to flat landscapes. However, there is no significant increase in firebrand landing distance when the FFDI is increased, particularly with rising temperatures. For flat terrain, the Q_{95} distance increases by 29% when the FDI rises from 40 to 60 based on wind speed and, by 21% when the FDI increases from 60 to 80. For hilly terrain, these increments are 70% and 24%, respectively, suggesting that firebrands tend to travel significantly further with increases in fire severity at lower FDI values (40 to 60) compared to higher FDI values (60 to 80). Figures S3(b) and S3(c) illustrate the normalized firebrand landing densities for flat and hilly terrains, respectively. Both scenarios clearly demonstrate that increasing wind speed causes firebrands to disperse further from the fire line rather than accumulate near the fire front. Consequently, the normalized firebrand density at specific locations particularly near the fireline decreases with higher FFDIs, while the likelihood of firebrands landing at greater distances increases. These findings underscore the critical influence of topography and FFDI varied by wind conditions on firebrand transport and the potential expansion of ignition risk zones.

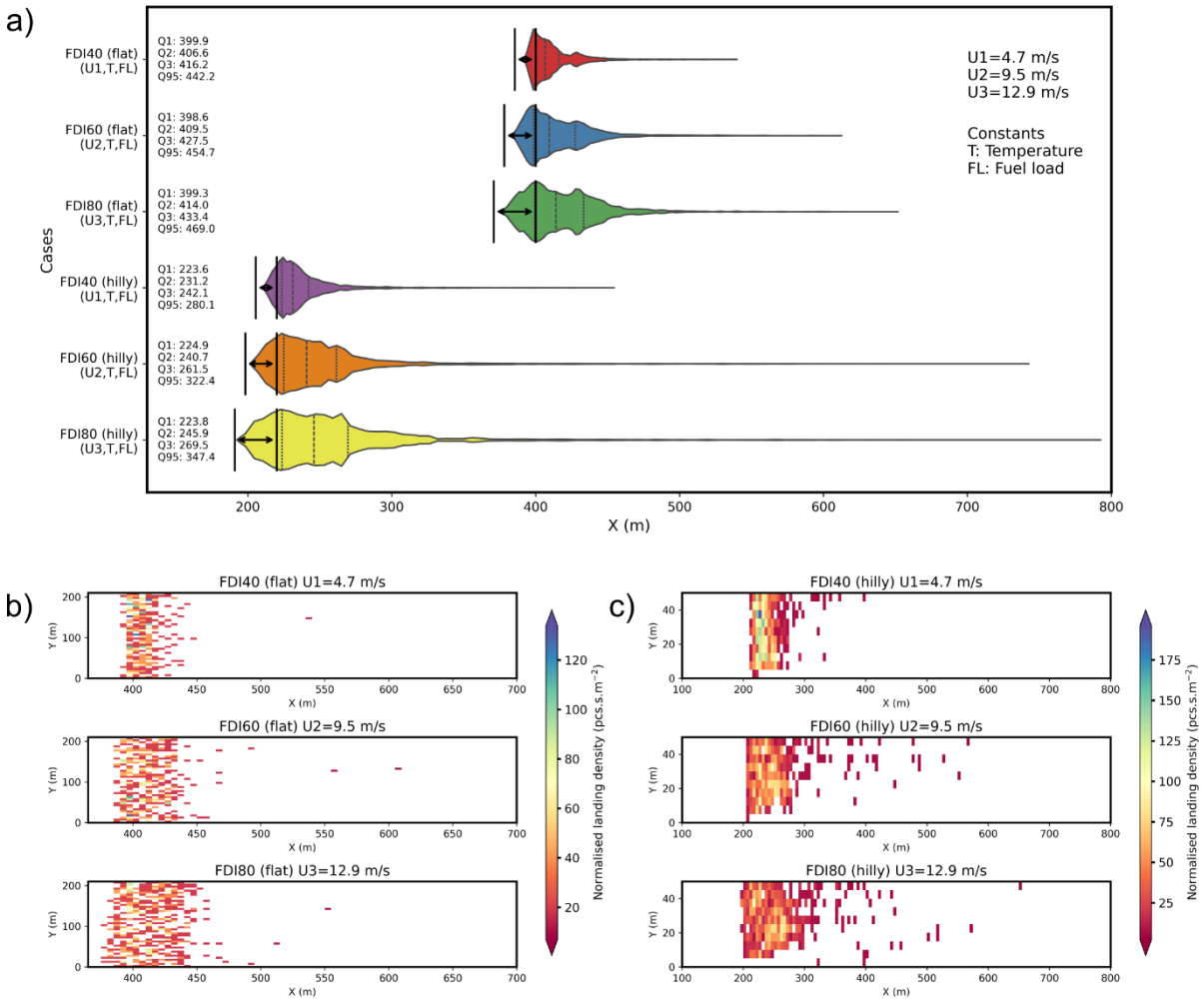

Figure S3- (a) Firebrand landing distance in flat and hilly terrains for selected FFDI by wind speed, with air temperature and fuel load held constant. Firebrand landing density, normalised to 1,000 generated firebrands, for selected FFDIs by wind speed, with temperature and fuel load held constant, in (b) flat terrain and (c) hilly terrain.

References

Australian Standard (2009) Construction of Buildings in Bush Fire Prone Areas (AS 3959). Sydney, Australia.

El Houssami M, Mueller E, Filkov A, Thomas JC, Skowronski N, Gallagher MR, Clark K, Kremens R, Simeoni A (2016) Experimental procedures characterising firebrand generation in wildland fires. *Fire Technology* **52**(3), 731-751.

McGrattan K, Hostikka S, McDermott R, Floyd J, Weinschenk C, Overholt K (2013) Fire dynamics simulator user's guide. *NIST special publication* **1019**(6), 1-339.

Noble I, Gill A, Bary G (1980) McArthur's fire-danger meters expressed as equations. *Australian journal of ecology* **5**(2), 201-203. doi:https://doi.org/10.1111/j.1442-9993.1980.tb01243.x